

Interlayer electrodynamic s in the organic superconductor (BED T TTF)₂Cu(NCS)₂: evidence for a transform ation w ithin the vortex state

S. Hill^Y

Department of Physics, University of Florida, Gainesville, FL 32611

M. M. Mola^Z

Department of Physics, Montana State University, Bozeman, MT 59717

J. S. Qualls

Department of Physics, Wake Forest University, Winston-Salem, NC 27109

(April 14, 2024)

A microwave cavity perturbation technique is used to probe the interlayer electrodynamic s within the vortex state of the organic superconductor (BED T TTF)₂Cu(NCS)₂. A Josephson plasma mode is observed which is extremely sensitive to correlations in the locations of vortices in adjacent layers and may, therefore, be used to gauge collective effects between vortices and crystal pinning sites in the title compound. Our previous investigations [M. M. Mola et al., Phys. Rev. B 62 (2000) 5965] revealed a transformation from a correlated quasi-two-dimensional pinned vortex phase, to either a depinned or liquid state. In this study, we carry out a detailed analysis of the magnetic field dependence of the Josephson plasma frequency within the two phases. Our findings agree favorably with recent theoretical models: within the liquid state, the squared plasma frequency (ω_p^2) decays with the inverse of the magnetic field strength, B ; whereas, in the pinned phase, a much slower decay is observed ($\omega_p^2 / B \propto B^{-0.35}$), which is indicative of weak pinning.

PACS numbers: 71.18.+y, 71.27.+a, 74.25.Nf

I. Introduction

The equilibrium magnetic field temperature phase diagram for type-II superconductors is extremely rich, including many different vortex solid, liquid and glassy phases [1,2]. Presently, the theory of vortex interactions in layered superconductors is incomplete, though much work has focused on this problem in recent years [1,2,3,4,5,6,7,8,9,10]. Information concerning vortex structure and dynamics is important for two reasons: first, the vortex structure contains important information regarding the symmetry of the superconducting state; second, vortex motion leads to dissipation, and an understanding of the dissipative mechanisms in superconductors is essential for progress in developing viable technology based on these materials. Superconducting vortices also provide an excellent laboratory for general phase-transition behavior [1]. Experimentally, all of the relevant parameters can be varied over wide ranges: the vortex density by many orders of magnitude by changing the magnetic field; thermal fluctuations by varying the temperature; pinning by varying disorder; and, in quasi-two dimensional (Q2D) systems, the coupling between the layers may be varied through the choice of material.

In the layered cuprate high temperature superconductors (HTS) and, more recently, in the Q2D organic superconductors (OS), it is widely accepted that Josephson coupling is responsible for the interlayer transport of Cooper pairs [11]. This adds to the complexity of the mixed state phase diagram — pancake vortices threaded by the same magnetic flux quantum may become completely decoupled from one layer to the next, creating a Q2D vortex state [1,2]. A model system for investigations of Q2D vortex physics, and one which has received relatively little attention in comparison with the HTS, is the 10 K organic superconductor $(\text{BEDT-TTF})_2\text{Cu}(\text{NCS})_2$, where BEDT-TTF denotes bis-ethylenedithio-tetrathiafulvalene [12,13]. Like the oxide HTS, $(\text{BEDT-TTF})_2\text{Cu}(\text{NCS})_2$ possesses a layered structure in which highly conducting BEDT-TTF planes are separated by insulating anion layers; for this material, the least conducting direction is along the crystallographic a axis [12]. The anisotropy parameter in the normal state, given by the ratio of the in-plane

to out-of-plane conductivities $\kappa_{bc} = \kappa_a$, is ~ 1000 . In the superconducting state, the anisotropy parameter is given by $\gamma = \kappa_c / \kappa_{ab} \sim 100 - 200$, where κ_c and κ_{ab} are the London penetration depths for AC currents induced parallel ($\kappa_{ab} \sim 0.8 \text{ } \mu\text{m}$) and perpendicular ($\kappa_c \sim 100 \text{ } \mu\text{m}$) to the conducting layers respectively [12,13,14,15]. Such a large anisotropy makes this OS a prime candidate to study Josephson coupling, and changes in this coupling upon the introduction of vortices into the sample, through the application of an external magnetic field. Unlike many of the HTS, this material is extremely clean, possessing far fewer crystal defects or pinning sites for magnetic flux. Furthermore, because of the reduced T_c and H_{c2} ($T_c = 10 \text{ K}$ and $\mu_0 H_{c2} = 4 \text{ tesla}$ for the field perpendicular to the layers), one can probe much more of the magnetic field-temperature parameter space within the superconducting state than is currently possible for the HTS [12,13].

Below T_c , a Josephson plasma resonance (JPR) dominates the interlayer (a-axis) electrodynamics of $(\text{BEDT-TTF})_2\text{Cu}(\text{NCS})_2$ [16,17,14,18]. The squared JPR frequency (ω_p^2) is directly proportional to the maximum interlayer (or Josephson) current density $J_m(B, T)$. In turn, $J_m(B, T)$ is related to the zero-field interlayer critical current density J_0 through the expression

$$J_m(B, T) = J_0 \hbar \cos'_{n,n+1}(r) i_t i_d; \quad (1)$$

where $\cos'_{n,n+1}(r)$ is the gauge-invariant difference in the phase of the superconducting order parameter between layers n and $n+1$ at a point $r = x, y$ in the bc plane, and $\hbar i_t$ and $\hbar i_d$ denote thermal and disorder averages [4]. $\cos'_{n,n+1}(r)$ depends explicitly on the vortex structure within the mixed state and is, thus, responsible for the field dependence of the JPR frequency ω_p . In the case of a 3D ordered flux-line-lattice, at $T = 0$, $\hbar \cos'_{n,n+1}(r) i_t i_d = 1$ and maximum Josephson coupling occurs. However, in the presence of any disorder, the flux lines will deviate from linearity and $\hbar \cos'_{n,n+1}(r) i_t i_d$ will be suppressed. Sources of disorder include: crystal defects, which create random vortex pinning sites; thermal fluctuations which may lead to a vortex lattice melting transition; or a 3D to 2D crossover transition, whereby the flux lines lose their rigidity, and the pancake vortices in adjacent

layers decouple. A comprehensive account of the influence of vortices and the role of disorder is beyond the scope of this article; the interested reader should refer to e.g. refs. [3,4,5,6].

In a previous investigation [14], we reported an unusual magnetic field dependence of the JPR frequency ω_p , which had been predicted for a weakly pinned Q2D pancake vortex phase. In addition, we identified a possible transformation from this pinned phase, to a liquid state, upon crossing the irreversibility line (high-B, high-T side) [14,15]. In this article, we extend the scope of these investigations. In particular: we carefully evaluate the field dependence of ω_p in the low B/T pinned phase, and compare our findings with detailed theoretical predictions; we carefully map out the phase boundary separating the pinned and liquid phases from measurements covering an extended frequency range (16–200 GHz); and we evaluate the field dependence of ω_p in the high temperature phase, and consider various models for this phase.

II. Experimental details

The high degree of sensitivity required for single crystal measurements is achieved using a resonant cavity perturbation technique in combination with a broad-band Millimeter-wave Vector Network Analyzer (MVNA) exhibiting an exceptionally good signal-to-noise ratio [19]. The MVNA is a phase sensitive, fully sweepable (8 to 350 GHz), superheterodyne source/detection system. Several sample probes couple the network analyzer to a range of high sensitivity cavities (Q factors of up to 25,000) situated within the bore of a 7 tesla superconducting magnet. Current capabilities allow single crystal measurements at any frequency in the range from 8 to 200 GHz, at temperatures down to 1.5 K (± 0.01 K), and for any geometrical combination of DC and AC field orientations up to 7 T (up to 45 T at the National High Magnetic Field Laboratory); this instrumentation is described in detail in ref. [19]. The use of a narrow band cavity offers many important advantages over non-resonant methods. Careful consideration concerning the coupling of radiation to and from the cavity (via waveguide), combined with the ability to study very small samples, eliminates problems associated with standing waves in the sample probe [19]. This, in turn, eliminates a

mixing of the dissipative and reactive responses of the sample under investigation and, when combined with a vector detection scheme, enables faithful extraction of both components of the complex conductivity. Finally, the use of a cavity enables positioning of a single crystal sample into a well defined electromagnetic field environment, i.e. the orientations of the DC and AC magnetic fields relative to the sample's crystallographic axes are precisely known. In this way, one can systematically probe each diagonal component of the conductivity tensor (in principle, the off-diagonal components also) [20].

Within the superconducting state, dissipation is governed by the surface resistance of the sample, i.e. the real part of the surface impedance $\hat{Z}_s = R_s + iX_s = (\hat{\sigma}_o)^{1/2}$ [20]. In this article, measurements are restricted to geometries which probe only the inter-layer electrodynamics; the precise details as to how we achieve this are described elsewhere [19,20]. Consequently, the measured dissipation depends only on the interlayer conductivity $\hat{\sigma}_a(B, T)$, which includes contributions from the Josephson tunneling of Cooper pairs and the normal quasiparticles. A simple two-fluid model leads to a surface impedance of the form

$$Z_s = \frac{v}{4\pi} \frac{\sigma_o + \frac{\omega_p^2}{\omega^2}}{\sigma_o + \frac{\omega_p^2}{\omega^2} + i\omega} ; \quad (2)$$

where $\gamma = \gamma_q$ is a damping term that depends only on the normal quasiparticle contribution to the conductivity, γ_q . Eq. (2) gives rise to an asymmetric JPR, as shown in Fig. 1. This particular simulation assumes ω_p^2 / B^2 , as determined from experiment (see section III). Furthermore, in order to reproduce the increased damping of the JPR with increasing field, as observed experimentally, we assume a quasiparticle conductivity which increases linearly with the flux density B . The data in Fig. 1 reproduce the main features observed from our previously published measurements of the JPR frequency dependence [14], i.e. the asymmetric resonance broadens and moves to higher field as the measurement frequency is reduced. The reason for the shift in the resonance position is discussed below.

While our simulations attribute the broadening and asymmetry of the JPR entirely to

quasiparticle damping effects, there does exist another possibility that has recently been discussed in the literature [21]. Inhomogeneous broadening of the JPR line, caused by random fluctuations in the interlayer Josephson coupling, has also been shown to produce asymmetry in the JPR line. We save a detailed discussion of this effect until the latter sections of this article. The main purpose of the simulation in Fig. 1 is to emphasize that the JPR asymmetry arises naturally from electrodynamics, i.e. the measured dissipation within the cavity is governed both by the real and imaginary parts of the complex conductivity [20]. Even if one assumes a field independent dissipative mechanism, the electrodynamics still result in an asymmetric JPR lineshape similar to the one shown in Fig. 1.

All microwave measurements were conducted in a mode where the measurement frequency is held constant (due to the narrow band technique), and the magnetic field is swept at different fixed temperatures, i.e., the field tunes ω_p , and a JPR is observed whenever $\omega_p(B, T)$ matches the measurement frequency ω . Application of a magnetic field generally suppresses the critical current density along the *a*-axis, thereby reducing ω_p . This is due to the fact that an increasing flux density, when combined with disorder and thermal fluctuations in the vortex positions, tends to suppress interlayer Josephson coupling. In a fixed frequency/swept field experiment, therefore, any external factors that increase ω_p (e.g. a change in temperature) will shift the observed JPR to higher magnetic field, since a stronger field will be required to shift $\omega_p(B)$ down to the measurement frequency ω . Conversely, any external factors which reduce ω_p will shift the JPR to lower field. This will be important for subsequent analysis of the temperature dependence of the JPR in the following section, and accounts for the shift in the resonance positions in Fig. 1, i.e. stronger fields are necessary to suppress ω_p to lower measurement frequencies.

Several different single crystals of $(\text{BEDT-TTF})_2\text{Cu}(\text{NCS})_2$, with approximate dimensions $0.75 \times 0.5 \times 0.2 \text{ mm}^3$, were used in this study; all of the samples were grown in the same batch using standard techniques [12]. We found that all samples gave qualitatively similar results. Temperature control was achieved using a Cernox thermometer and a small resistive heater attached mechanically to the cavity [19]. DC magnetic fields were applied parallel to

the sample's a-axis for all measurements, and field sweeps were made at a constant rate of approximately 1 T per minute.

III. Results and discussion

Figure 2 shows temperature dependent microwave dissipation (ω/R_S) for two different frequencies: a) 111 GHz and b) 134 GHz. The JPR is observed as a broad asymmetric resonance (see Fig. 1 for comparison) with a strongly temperature dependent amplitude and width. For these two frequencies, the resonance peak position exhibits a non-monotonic dependence on temperature. The top traces in each figure were obtained at the lowest temperature (2 K), and the bottom traces at the highest temperature (10 K) (see figure caption for the exact temperatures). As noted above, $J_m(B, T)$ and, therefore ϕ_p , is suppressed upon application of a magnetic field, i.e. the JPR at the lower frequency of 111 GHz is observed at higher fields. The higher field 111 GHz resonances are also broader, as noted in the previous section. Figure 3 plots the resonance positions, as a function of temperature, for measurements at several different frequencies. The data clearly define a line (dashed curve) separating two regimes, one for which $\partial\phi_p/\partial T < 0$, the other for which $\partial\phi_p/\partial T > 0$. Similar behavior has been observed in $\text{Bi}_2\text{Sr}_2\text{CaCu}_2\text{O}_{8+x}$ [7,8]. We note from above that a resonance which moves to lower fields implies a reduction in ϕ_p , and vice versa.

Observation of a region of field/temperature parameter space for which $\partial\phi_p/\partial T > 0$, implies that Josephson coupling is enhanced upon raising the temperature. Or, phrased in another way, this implies that raising the temperature results in an increased correlation in the positions of pancake vortices in adjacent layers. This rather counter-intuitive result can only be understood in terms of a vortex state which exhibits some degree of pinning [4,22]. It is already well established that the 3D flux-line-lattice decouples at relatively weak fields on the order 10 mT [23]. However, the nature of the subsequent vortex state has not been well established, since the loss of a 3D ordered state renders most techniques (e.g. SR [23]) insensitive to any remaining long range order within the layers. One possible reason for the enhancement in the quantity $\hbar\omega\cos'_{n,m+1}(r)\phi_{\text{td}}/\phi_p$, upon increasing the temperature,

is illustrated by means of the schematic in Fig. 4. Vortex-vortex ($1/r$) interactions result in intra-layer correlations in the locations of vortices within each particular layer. A Q 2D hexagonal vortex lattice (as depicted in Fig.4) represents a limiting case of this correlated state, though a Q 2D glassy state probably offers a more realistic description of the apparent pinned vortex phase discussed here. Defects (not shown) pin a small fraction of the vortices. Since the intra-layer vortex-vortex interactions overwhelm the interlayer Josephson coupling at fields above the decoupling field (few mT), collective pinning has the effect of locking the positions of vortices in one layer independently of the positions of the vortices in adjacent layers. Consequently, pancake vortices in layers n and $n+1$, which are threaded by the same flux quantum, do not necessarily occupy the same position in the xy plane. This leads to a finite separation ($r_{n,n+1}$) of the xy -coordinates of vortices in layers n and $n+1$, and contributes to a suppression of $h\phi_{0,n,n+1}(r)i_{t,i_d}$. Interlayer Josephson coupling provides a weak restoring force which acts to restore linearity among the pancake vortices. The combined potentials due to inter-vortex repulsion (deep narrow minimum in Fig. 4b dashed curve) and Josephson coupling (broad shallow minimum in Fig. 4b dashed curve), results in an asymmetric (anharmonic) potential minimum (solid curve in Fig. 4b) for the separation, $r_{n,n+1}$, between vortices in layers n and $n+1$. One can now see that increased thermal fluctuations will lead to a reduction in $h\phi'_{n,n+1}(r)i_{t,i_d}$ and, hence, an increase in $h\phi_{0,n,n+1}(r)i_{t,i_d}$, i.e. thermal fluctuations lead to increased linearity of the flux lines.

One other possible explanation for the $\partial I_p / \partial T > 0$ behavior, which has been discussed by Matsuda et al. in connection with JPR measurements on $Bi_2Sr_2CaCu_2O_{8+x}$ [22], involves a non-equilibrium critical state. We note that the existence of a critical state implies collective pinning and glassy behavior, i.e. pinning plus intra-layer vortex correlations. In this picture, in-plane currents associated with the critical state exert Lorentz forces on the pancake vortices. For situations in which the interlayer Josephson coupling is weak, as is the case in our experiments, the Lorentz forces drive the pancake vortices out of alignment in a somewhat analogous fashion to the collective pinning scenario discussed above. Consequently, inter-layer coherence is suppressed. Furthermore, this suppression of $h\phi'_{n,n+1}(r)i_{t,i_d}$ increases

upon lowering the temperature, since the in-plane critical currents increase with decreasing temperature. Field cooled experiments offer a means of distinguishing between these two scenarios. However, for the purpose of this article, we note that both explanations result in the same conclusions concerning the nature of the vortex state in the regions of Fig. 3 where $\partial \rho_p / \partial T > 0$.

Having established the existence of a Q2D pinned vortex phase over a considerable portion of the mixed state phase diagram for the title compound, one next has to consider the reasons for a crossover in the temperature dependence of the JPR frequency (dashed line in Fig. 3). $\partial \rho_p / \partial T < 0$ implies a decreasing interlayer coherence with increasing temperature. The first possible explanation is a melting or glass transition [9,10,24,25], whereby thermal or quantum induced fluctuations in the positions of the pancake vortices become comparable to the average in-plane inter-vortex separation [26]. In this scenario, pinned vortices may remain pinned; however, long range order among the vortices is completely lost. The result is a Q2D flux liquid state in which inter-vortex repulsion plays a much reduced role. Nevertheless, the liquid state may exhibit some residual viscosity due to the residual inter-vortex interactions between mobile and pinned vortices [2]. The transition may be expressed in terms of either a temperature dependent critical field, $B_m(T)$, or as a field dependent critical temperature, $T_m(B)$. Once the fluctuations in the positions of pancake vortices become large in comparison to the average in-plane vortex separation [i.e. $T > T_m(B)$ or $B > B_m(T)$], the model described above to explain $\partial \rho_p / \partial T > 0$ breaks down (see Fig. 4). In this limit, increased thermal fluctuations serve only to suppress $\hbar \cos'_{n,m+1}(r) i_{td}$; hence, the observed temperature dependence of ρ_p .

A subtly different explanation for the observed crossover in the temperature dependence of the JPR frequency (dashed line in Fig. 3) involves a depinning transition [27,28]. In this picture, pinning forces are considerably weaker than the inter-vortex repulsive forces that stabilize the correlated state. Upon raising the temperature, vortices execute larger and larger collective displacements from equilibrium. In fact, this collective behavior would be indistinguishable from the picture described above to explain $\partial \rho_p / \partial T > 0$ (see Fig. 4),

i.e. the collective fluctuations would lead to an increase in $\langle \cos'_{n,n+1}(r) \rangle_{\text{ld}}$, as observed for $T < T_m(B)$. Upon exceeding a critical depinning threshold (characteristic of the nature of the pinning), the vortex arrays become completely depinned or mobile. The result is a depinned or mobile Q2D vortex state in which pinning forces play a much reduced role. As in the liquid case, the depinned phase may be expected to exhibit a finite viscosity due to the weak residual interaction with pinning centers. Furthermore, once the collective displacements of the vortices exceed the average in-plane vortex separation, one expects the temperature dependence of ρ_p to crossover in the same way as described above for the glass/liquid transition.

To reiterate, the glass/liquid and depinning transitions seem to describe qualitatively similar phenomena. However, the physical origin of each transition is rather different. In the former case, thermal fluctuations overcome the inter-vortex interactions that maintain correlations among vortices within each layer, while in the depinning case, thermal fluctuations overcome the pinning forces and the correlated flux bundles become mobile. Unfortunately, because the JPR frequency depends only on the averaged value of the $\cos'_{n,n+1}(r)$, it is only sensitive to global changes in the critical current density, and not the mechanisms for such changes. However, for either case mentioned above, the opposing temperature dependence observed above and below the transition temperature $T_m(B)$, should be expected.

Having identified a transformation in the vortex structure from the temperature dependence of the JPR frequency, we next turn our attention to the field dependence of ρ_p in each phase. Our previous efforts to plot ρ_p versus B were complicated by the fact that insufficient data were obtained completely within each of the phases [14], i.e. much of the data straddled the transition line. Various theoretical models predict quite different behavior for ordered and disordered phases, as well as a strong dependence on the nature of the pinning. Recently, A.E. Koshelev has derived the explicit form of ρ_p within the Q2D vortex liquid state, using field theoretical methods [6]:

$$\rho_p^2 = \frac{4}{\mu_0} \frac{dJ_o^2}{dB} ; \quad (3)$$

here, d is the interlayer separation, and ϕ_0 is the flux quantum. Consequently, within the Q2D vortex liquid state, the JPR frequency should follow a $\omega_p^2 / 1 = TB$ dependence. To this end, ω_p^2 is plotted as a function of applied field in Fig. 5. These data points were all obtained at 7 K and at fields above the transition field $B_m(T)$, i.e. in the disordered state. The solid line is a powerlaw fit of the form $\omega_p^2 = AB^\alpha$, with $\alpha = 0.93 \pm 0.05$. Since this value is close to unity, it supports the assumption that the system is in a highly disordered, or liquid-like state. The value of $J_0 = 2 \times 10^7 \text{ A m}^{-2}$ obtained from the fit is in excellent agreement with the value obtained from previous investigations [14].

Within the low- T /low- B phase, determination of the field and temperature dependence of the resonance frequency gives insight into the nature of the pinning [3,4]. Like the vortex liquid state, the JPR frequency is expected to follow a powerlaw dependence, with an exponent that tends to unity with increasing disorder. A reduction in the number of pinning centers in cleaner crystals results in a better alignment of the pancake vortices. This, in turn, leads to a reduction in the magnitude of the exponent in the powerlaw, i.e. to a much slower suppression of ω_p with field. Fig. 6 plots the field dependence of the JPR frequency for data obtained entirely within pinned vortex glass phase, i.e. for fields below the transition field $B_m(T)$. The solid curve is a powerlaw fit to the data, from which an exponent of $\alpha = 0.35 \pm 0.02$ is obtained, indicative of an intermediate to low degree of pinning within this phase. We note that similar experiments on several HTS compounds also show a powerlaw behavior, with exponents of order unity in every case [7,8]. This is seen even within the ordered vortex solid state, indicating that the materials studied here are considerably cleaner than typical HTS materials, something which has been well established via a range of other techniques. Batch-to-batch variations in sample quality have, however, been noted for this compound. For example, there is no overlap between the data in Fig. 6 and data from Fig. 5 of ref. [14], which were obtained for a sample from a different synthesis. Furthermore, several other groups have published JPR data for the title compound, and there is rarely good agreement between the JPR peak positions for a given frequency and temperature [16,17,18,29].

Finally, we comment on the linewidth and shape of the JPR. While the model discussed in ref. [21] (involving inhomogeneous broadening due to random Josephson coupling – see also [32]), accounts for the observed asymmetry of the JPR, it cannot account for the field dependence of the JPR widths observed from our measurements. In particular, this model predicts a linewidth which is inversely proportional to magnetic field strength. Examination of Figs 2a) and b) reveal a completely opposite trend. Indeed, the JPR width is approximately proportional to B , i.e. the data in Fig. 6a), which are observed at roughly twice the field strength of the data in Fig. 6b), span approximately twice the field window of the data in Fig. 6b). This trend is even more apparent from our earlier studies (see e.g. Fig. 2 of ref. [14]). Although we cannot completely rule out an inhomogeneous contribution to the linewidths, the pronounced broadening of the JPR with field suggests that quasiparticle damping effects dominate both the linewidths and shapes.

IV. Summary and conclusions

We have utilized a resonant cavity perturbation technique to probe the interlayer electrodynamics of the Q2D $(\text{BEDT-TTF})_2\text{Cu}(\text{NCS})_2$ organic superconductor. A JPR is observed, which proves to be extremely sensitive to correlations in the locations of vortices in adjacent layers. By following the temperature and field dependence of JPR frequency (ν_p) at many frequencies, a clear transition line emerges near the irreversibility line, where a first order phase transition has also been observed from magnetic measurements [33]. A global mixed state phase diagram, which includes this data, has recently been published in refs. [15,30]. Below the transition line $B < B_m(T)$ [or $T < T_m(B)$], the existence of a correlated Q2D vortex (glassy) phase has been established. Two possibilities have been considered for the vortex transformation that takes place at $B_m(T)$ – namely, melting and depinning transitions. In either scenario, the high- B /high- T state resembles a liquid-like state (up to H_{c2}). In the melting scenario, residual inter-vortex interactions cause some remnant local order or clustering of vortices around pinning sites, but longer range correlations are suppressed [2]. Under the depinning scenario, finite vortex correlations exists; however, the 2D vortex

arrays may break up into domains or flux bundles, with some still pinned, while others are mobile. This represents a so-called vortex slush phase. Similar plastic flows of vortices have been observed in the HTS [31]. Essentially, the vortex slush and the pinned liquid are the same, with the subtle difference being the inter-vortex correlation length, i.e. the sizes of the pinned and mobile domains is much larger for the slush than for the pinned liquid. It is clear from these investigations, that organic superconductors offer the opportunity to investigate a distinctly different pinning regime from the more widely studied HTS materials.

V. Acknowledgements

This work was supported by the National Science Foundation (DMR0196461 and DMR0196430). S.H. is a Cottrell Scholar of the Research Corporation.

VI. References cited

^y email: hill@phys.u.edu

^z Permanent address: Humboldt State University, Department of Physics, Arcata, CA 95521

- [1] G.W. Crabtree and D.R. Nelson, Physics Today, April 1997.
- [2] G. Blatter, M.V. Feigel'man, V.B. Geshkenbein, A.I. Larkin, V.M. Vinokur, Rev. Mod. Phys. 66, 1125 (1995).
- [3] L.N. Bulaevskii, M.P. Maley, and M. Tachiki, Phys. Rev. Lett. 74, 801 (1995).
- [4] L.N. Bulaevskii, V.L. Pokrovsky, M.P. Maley, Phys. Rev. Lett. 76, 1719 (1996).
- [5] A.E. Koshelev, Phys. Rev. Lett. 77, 3901 (1996).
- [6] A.E. Koshelev, L.N. Bulaevskii, M.P. Maley, Phys. Rev. Lett. 81, 902 (1998).
- [7] O.K.C. Tsui, N.P. Ong, Y. Matsuda, Y.F. Yan, J.N. Peterson, Phys. Rev. Lett. 73, 724 (1994).

- [8] Y .M atsuda, M .B .G aifullin, K .K umagai, K .K adowaki, T .M ochiku, Phys.Rev.Lett. 75, 4512 (1995).
- [9] E . Zeldov, D .M ajer, M .K onczykowski, V .B .G eshkenbein, V .M .V inokur, H . Shtrikman, Nature (London) 375, 373 (1995).
- [10] A .Schilling, R .A .F isher, N .E .Phillips, U .W elp, D .D asgupta, W .K .K wok, G .W .C rabtree, Nature (London) 382, 791 (1996).
- [11] R .K leiner and P .M üller, Phys.Rev.B 49, 1327 (1994).
- [12] T .Ishiguro, K .Yamaji, and G .Saito, Organic Superconductors, Springer-Verlag (Berlin, 1998).
- [13] J .Singleton, Rep.Prog.Phys. 63, 1111 (2000).
- [14] M .M .M ola, J .T .K ing, C .P .M cRaven, S .H ill, J .S .Q ualls, J .S .B rooks, Phys.Rev.B 62, 5965 (2000).
- [15] M .M .M ola, S .H ill, J .S .B rooks, J .S .Q ualls, Phys.Rev.Lett. 86, 2130 (2001).
- [16] T .Shibauchi, M .Sato, S .O oi, and T .Tam egai, Phys.Rev.B 57, R5622 (1998).
- [17] T .Shibauchi, M .Sato, A .M ashio, T .Tam egai, H .M ori, S .Tajima, and S .Tanaka, Phys.Rev.B 55, R11 977 (1997).
- [18] S .H ill, N .Harrison, M .M ola, and J .W osnitza, Phys.Rev.Lett. 86, 3451 (2001)
- [19] M .M ola, S .H ill, M .G ross, and P .G oy, Rev.Sci.Instrum .71, 186 (2000), and references therein.
- [20] S .H ill, Phys.Rev.B 62, 8699 (2000).
- [21] A .E .K oshelev and L .N .B ulaevskii, Phys.Rev.B 60, R3743 (1999).
- [22] Y .M atsuda et al, Phys.Rev.Lett. 78, 1972 (1997).
- [23] S .L .Lee, F .L .P ratt, S .J .B lundell, C .M .A egerter, P .A .P atenden, K .H .C how, E .Forgan, T .Sasaki, W .Hayes, H .K eller, Phys.Rev.Lett. 79, 1563 (1997).

- [24] A . Houghton, R A . Pelcovits, and A . Sudb, Phys. Rev. B 40, 6763 (1989).
- [25] L . Fruchter, A . Aburto, and C . Pham -Phu, Phys. Rev. B 56, 2936 (1997).
- [26] F . Lindem ann, Z . Physik, (leipzig) 11, 69 (1910).
- [27] N . Lutke-Entrup, B . Placais, P . Mathieu, and Y . Simon, Phys. Rev. Lett. 79, 2538 (1997).
- [28] V . I. Marconi and D . Dom inguez, Phys. Rev. Lett. 82, 4922 (1999).
- [29] J M . Schram a, E . Rzepniewski, R . S. Edwards, J. Singleton, A . Ardavan, M . Kum oo, and P . Day, Phys. Rev. Lett. 83, 3041 (1999).
- [30] C . M ielke, J. Singleton, M -S . Nam , N . Harrison, C C . Agosta, B . Fravel, L . K . M ontgom ery, cond-m at/0103501.
- [31] A . P . Reyes, X . P . Tang, H . N . Bachm an, W . P . Halperin, J . A . M artindale, P . C . Ham mel, Phys. Rev. B 55, R14 737 (1997).
- [32] L . N . Bulavskii, D . Dom inguez, M . P . M aley, A . R . Bishop, O . K . T sui, N . P . Ong, Phys. Rev. B 54, 7521 (1996).
- [33] M . Inada, T . Sasaki, T . N ishizaki, N . K obayashi, S . Yam ada, T . Fukase, J . Low Temp . Phys. 117, 1423 (1999).

Figure captions

Fig. 1. Simulations of the frequency and magnetic field dependence of the surface resistance given by Eq. (2). The asymmetric peak is due to the JPR.

Fig. 2. Temperature dependence of the field dependent microwave dissipation observed at a) 111 GHz and b) 134 GHz. The asymmetric peak is due to the JPR (see Fig. 1 for comparison). The temperatures in each figure are, from top to bottom (in kelvin): 2.0, 2.2, 2.5, 2.7, 3.1, 3.2, 3.5, 3.7, 4.0, 4.2, 4.5, 4.7, 5.0, 5.2, 5.5, 5.7, 6.0, 7.0, 8.0, 9.0.

Fig. 3. A compilation of the temperature dependence of the peak positions of the JPR observed at several different frequencies (indicated in the figure). The dashed line separates regions with different temperature dependencies for ω_p .

Fig. 4 a) Schematic representing a Q2D vortex solid, in which long range hexagonal order exists within each layer, yet there is no correlation in the locations of vortices in adjacent layers, even though they may be threaded by the same flux quantum. b) The resultant potential $U(r_{n,m-1})$ (solid line) for a vortex in layer $n-1$ subjected to a deep potential minimum (dashed curve) due to the rigidity of the vortex lattice in that layer, and a weaker offset potential minimum (due to the interlayer Josephson coupling) which acts to line up pancake vortices threaded by the same flux quantum.

Fig. 5. Magnetic field dependence of the squared JPR frequency within the depinned or liquid state ($T = 7$ K). The solid line is a powerlaw fit to the data.

Fig. 6. Magnetic field dependence of the squared JPR frequency within the weakly-pinned Q2D ordered/glassy phase ($T = 2$ K). The solid curve shows the fit to a powerlaw [Eq. (3)].

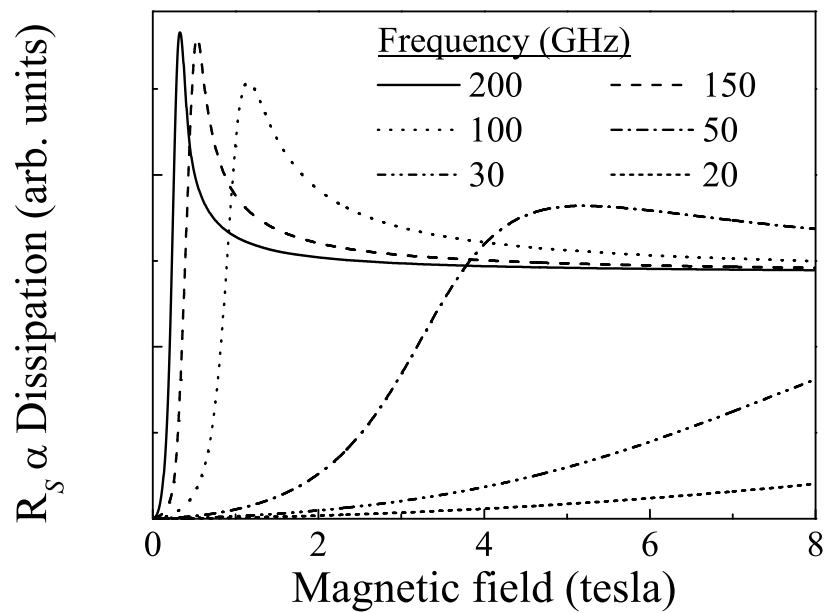


FIG .1. Hillet al.

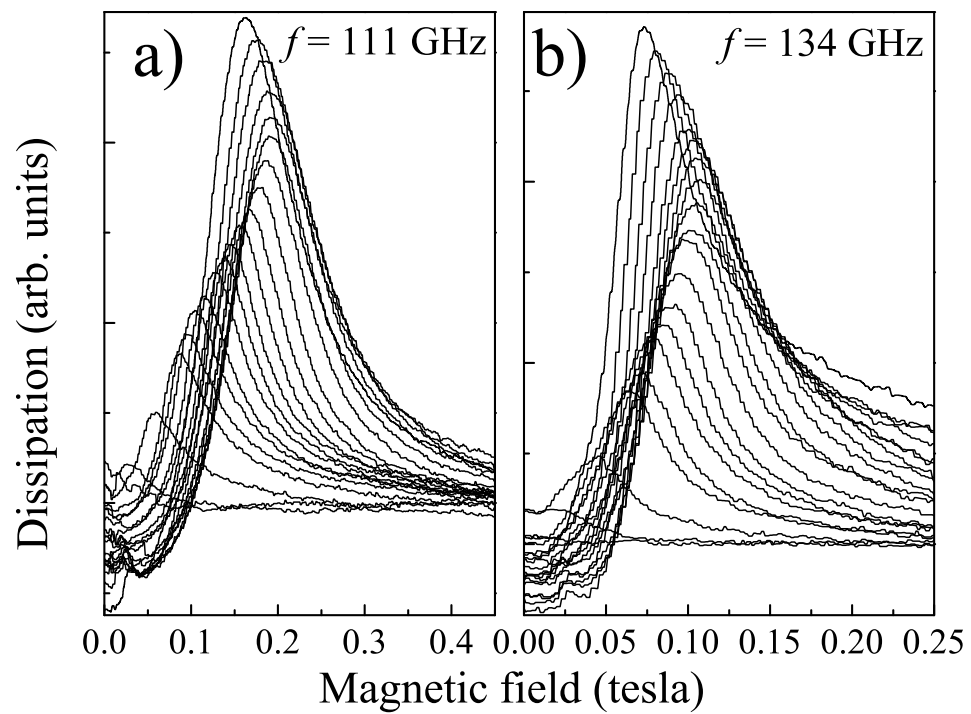


FIG .2. Hill et al.

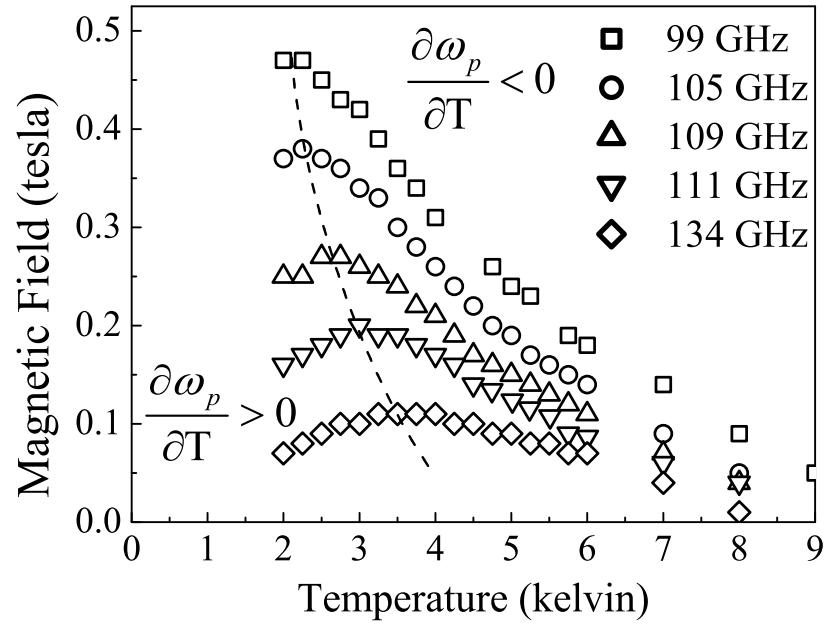


FIG .3. Hill et al.

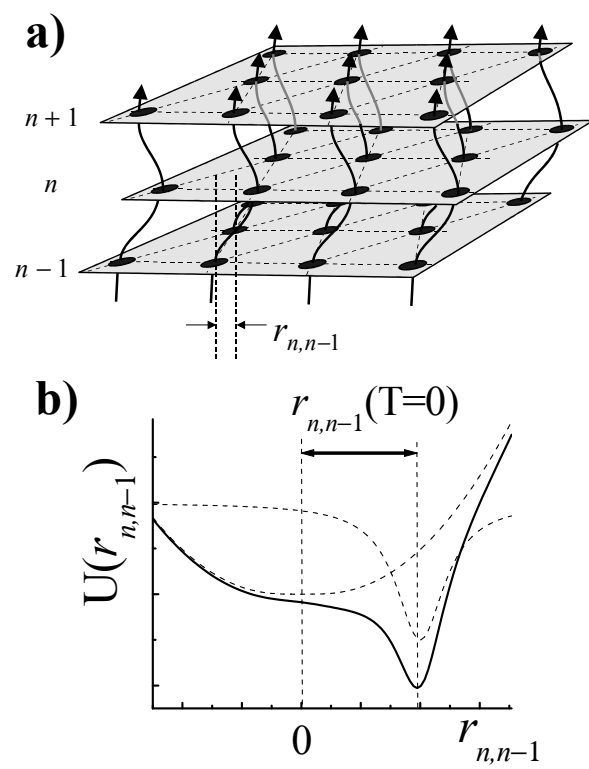


FIG . 4. Hill et al.

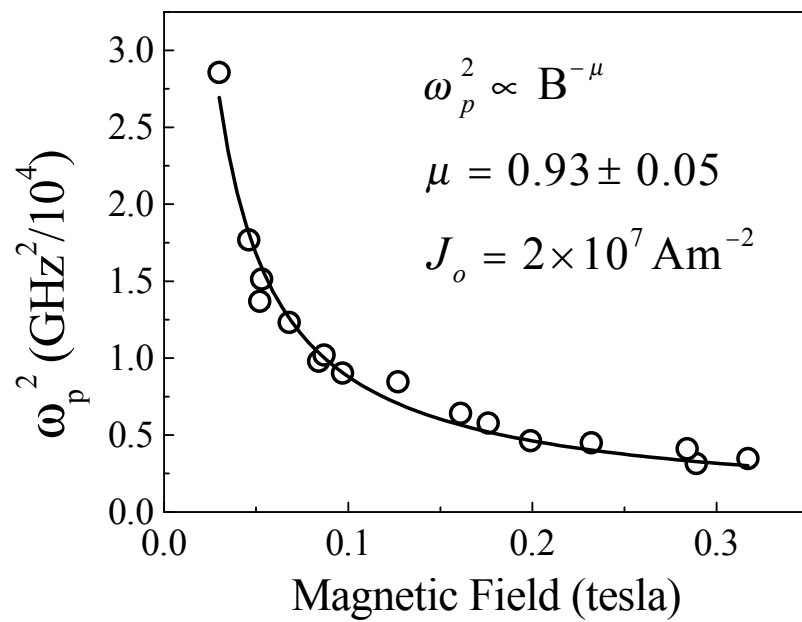


FIG .5. Hill et al.

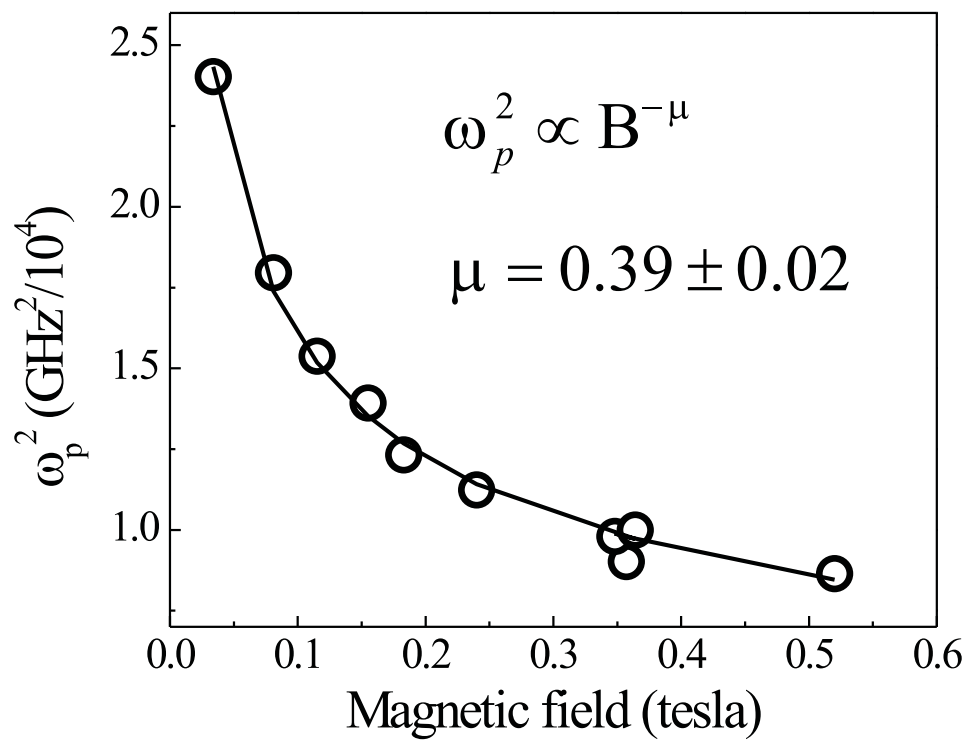


FIG . 6. Hill et al.